Journal of Electrocardiology 53 (2019) 18–27

Contents lists available at ScienceDirect

Journal of Electrocardiology

journal homepage: www.jecgonline.com

Temporal stability and specificity of high bipolar electrogram entropy regions in sustained atrial fibrillation: Implications for mapping

Dhani Dharmaprani, B.Eng(Hons) [a], Andrew D. McGavigan, MD [a,b], Darius Chapman [c], Rayed Kutlieh, B.Eng(Hons) [d], Shivshankar Thanigaimani [a], Lukah Dykes [a], Jonathan Kalman [e], Prashanthan Sanders [c,h], Kenneth Pope, PhD [f], Pawel Kuklik, PhD [g], Anand N. Ganesan, MBBS PhD [a,b,*]

[a] College of Medicine and Public Health, Flinders University of South Australia, Adelaide, SA, Australia
[b] Department of Cardiovascular Medicine, Flinders Medical Centre, Adelaide, SA, Australia
[c] University of Adelaide, Adelaide, SA, Australia
[d] Abbott, Adelaide, SA, Australia
[e] Royal Melbourne Hospital, Melbourne, Vic, Australia
[f] College of Science and Engineering, Flinders University of South Australia, Adelaide, SA, Australia
[g] Department of Cardiology, University Medical Centre, Hamburg, Germany
[h] South Australian Health and Medical Research Institute, Adelaide, Australia

ARTICLE INFO

Available online xxxx

Keywords:
Atrial fibrillation
Mapping
Entropy
Information theory
Signal processing

ABSTRACT

Background: The potential utility of entropy (En) for atrial fibrillation (AF) mapping has been demonstrated in previous studies by multiple groups, where an association between high bipolar electrogram (EGM) entropy and the pivot of rotors has been shown. Though En is potentially attractive new approach to ablation, no studies have examined its temporal stability and specificity, which are critical to the application of entropy to clinical ablation. In the current study, we sought to objectively measure the temporal stability and specificity of bipolar EGM entropy in medium to long term recordings using three studies: i) a human basket catheter AF study, ii) a tachypaced sheep AF study and iii) a computer simulation study.

Objective: To characterize the temporal dynamics and specificity of Approximate, Sample and Shannon entropy (ApEn/SampEn/ShEn) in human (H), sheep (S), and computer simulated AF.

Methods: 64-electrode basket bi-atria sustained AF recordings (H:15 min; S:40 min) were separated into 5 s segments. ShEn/ApEn/SampEn were computed, and co-registered with NavX 3D maps. Temporal stability was determined in terms of: (i) global pattern stability of En and (ii) the relative stability the top 10% of En regions. To provide mechanistic insights into underlying mechanisms, stability characteristics were compared to models depicting various propagation patterns. To verify these results, cross-validation was performed across multiple En algorithms, across species, and compared with dominant frequency (DF) temporal characteristics. The specificity of En was also determined by looking at the association of En to rotors and areas of wave cross propagation.

Results: Episodes of AF were analysed (H:26 epochs, 6040 s; S:15 epochs, 14,160 s). The global pattern of En was temporally unstable (CV- H:13.42% ± 4.58%; S:14.13% ± 8.13%; Friedman- H: $p > 0.001$; S: $p > 0.001$). However, within this dynamic flux, the top 10% of ApEn/SampEn/ShEn regions were relatively temporally stable (Kappa >0.6) whilst the top 10% of DF regions were unstable (Kappa <0.06). In simulated AF scenarios, the experimental data were optimally reproduced in the context of an AF pattern with stable rotating waves surrounded by wavelet breakup (Kappa: 0.610; $p < 0.0001$).

Conclusion: En shows global temporal instability, however within this dynamic flux, the top 10% regions exhibited relative temporal stability. This suggests that high En regions may be an appealing ablation target. Despite this, high En was associated with not just the pivot of rotors but also with areas of cross propagation, which suggests the need for future work before clinical application is possible.

Abbreviations: AF, Atrial fibrillation; ShEn, Shannon entropy; ApEn, Approximate entropy; SampEn, Sample entropy; DF, Dominant Frequency.

* Corresponding author at: College of Medicine and Public Health, Flinders University, Flinders Drive, Bedford Park, SA 5042, Australia.
E-mail address: anand.ganesan@flinders.edu.au (A.N. Ganesan).

https://doi.org/10.1016/j.jelectrocard.2018.11.014

Introduction

Ablation outcome in persistent atrial fibrillation (AF) is a key area requiring improvement, with studies reporting the maintenance of sinus rhythm in <50% of patients following a single ablation procedure [1]. From this, it is clear that new approaches to human AF mapping are required [2,3].

To date, a limitation of many of the emerging mapping approaches is that they have utilised internal or company-specific proprietary technology algorithms [4]. The paucity of externally verifiable algorithms has had important consequences for reproducibility and independent validation, and has led to growing scepticism regarding the viability of individual patient-level mapping in the AF ablation field [5]. In multiple instances, initially promising single-centre ablation results using novel mapping strategies [6,7] have been unable to be replicated in independent mapping studies [8] or well-conducted randomized controlled trials [9,10]. In this context, there remains a compelling case for rigorously performed, mechanistically-based, open-source signal analysis and mapping studies to improve mechanistic understanding of AF dynamics, to in turn improve ablation outcomes.

To address this, the use of an information theoretic measure known as entropy has recently been explored in AF applications to map rotors and provide insights into bipolar electrogram (EGM) signal properties [11]. The reasoning behind this is: i) experimental studies have suggested rotors as a potential AF driver [12–15], ii) entropy is well established outside of cardiology and is commonly utilised to provide insights into the dynamics of biological systems, with uses such as anaesthesia monitoring [16] and for the detection of epilepsy [17], and iii) entropy algorithms are open source, which may resolve the issue of reproducibility. In addition, bipolar electrograms are the most commonly used recording modality in clinical electrophysiology, making these signals readily available for entropy analysis whilst also providing a direct and interpretable translation to what is seen clinically. Lastly, high bipolar electrogram Shannon entropy (ShEn) has been demonstrated by our group to be associated with the pivot of rotors [4,18,19], and subsequently entropy-based identification of the rotor pivot has been independently observed by multiple groups using a variety of entropy-based approaches, and in multiple model systems [20–25].

Although the association of high entropy to the rotor pivot has undergone rigorous validation, application of entropy-based approaches to clinical ablation is reliant on two current gaps in literature: i) the temporal characteristics of entropy and ii) the specificity of high entropy. Specifically, temporal stability determines whether high entropy regions are long standing and appearing consistently in the same regions, which would allow targeted ablation. On the other hand, specificity of high entropy determines whether these areas occur at only the pivot of rotors, or also other wave propagation patterns. The presence of both stability and specificity is critical to the feasibility of employing entropy for clinical AF ablation.

To address these gaps, our aim was to explore the temporal characteristics and specificity of entropy using three studies: i) a medium-duration human basket catheter AF study, ii) a long-duration tachypaced sheep basket study, and ii) a computational AF study. These studies investigate the temporal stability of bipolar EGM entropy using three entropy-based measures of information content, Approximate Entropy (ApEn), Sample Entropy (SampEn), and Shannon entropy (ShEn), applied to bipolar electrograms in prolonged recordings (≥5 min) in human and (≥20 min) animal experimental AF. To provide further insights into the potential AF mechanism responsible for the temporal characteristics seen in human and sheep models, we performed a computer simulation study to observe stability patterns in varying wave propagation scenarios.

Methods

Data acquisition

Human AF recordings

The vast majority of mapping studies available presently explore EGM properties using sequential AF mapping. However, a limitation of this approach is that it is limited by the inherent spatiotemporal stability of AF. Stable basket recordings can overcome this issue, and provides a means to assess the medium to long term temporal characteristics of electrograms [26].

Patients ($n = 12$) undergoing ablation for AF were recruited. Patients provided written informed consent with study approval by the Southern Adelaide Local Health Network Human Research Ethics Committee. 64-electrode basket catheters (Constellation, Boston Scientific, MA, 48 mm (4 mm spacing), 60 mm (5 mm spacing)) were utilised, based on pre-procedural computed tomographic scan atrial dimensions. Bipolar electrogram recordings [27] were obtained in spontaneous or induced AF lasting at least 5 min, similar to the protocol of Habel et al. [26]. For cases of induced AF, fibrillation was induced through rapid atrial pacing from the coronary sinus. 5-min recordings were taken in the anterior left atrium (LA), posterior LA and right atrium (RA). Anatomical stability was verified by regular fluoroscopic visualization, and in NavX (Abbott, IL, USA). Signals were filtered from 30 Hz to 500 Hz with a sampling rate of 1000 Hz using the Bard EP system (Laboratory System Pro, Boston Scientific, MA).

Sheep AF recordings

Right atrial tachypacing (16 weeks, (≥300 beats per minute) was used to obtain persistent AF. An electrophysiology study was undertaken under general anaesthesia using a 64-electrode constellation catheter (48 mm). Bipolar electrograms were filtered from 30 Hz to 500 Hz, and sampled at 1000 Hz. For each sheep, ≥20 min of intracardiac data were obtained in the left and right atrium.

Computer simulations

To provide further insight into the AF mechanisms underlying the human and animal entropy temporal characteristics, results via the kappa statistic and Friedman test *p*-values were compared to computational AF simulations demonstrating varying wave propagation patterns. Computer simulations were carried out on two-dimensional, isotropic, square grids (80×80) based on the Tusscher-Panfilov model [28]. Extracellular EGM calculations are detailed in Supplement S1.

To determine the specificity of high entropy, multiple AF-type scenarios demonstrating regions of repetitive wave cross propagation were simulated and analysed to test their association to high entropy. Specifically, these regions were defined as areas where waves pass from a multitude of directions, causing bipoles to experience an uncertainty in wavefront activation direction similar to what would be seen at the pivot of a rotor (Fig. 1).

Signal processing

Export and segmenting

Bipolar EGM were cleaned for low amplitude signals using Welch's power spectral density [29] (Supplement S4) to ensure low contact signals were not used in analyses. This was cross-validated using manual annotation. The remaining signals were then windowed into 5 s (5000 ms) segments; a temporal resolution used in previous literature [26].

Entropy and dominant frequency analysis

Entropy is an information theoretic approach that measures information content. As information can alternatively be thought of as the amount of uncertainty that is resolved, measuring this uncertainty

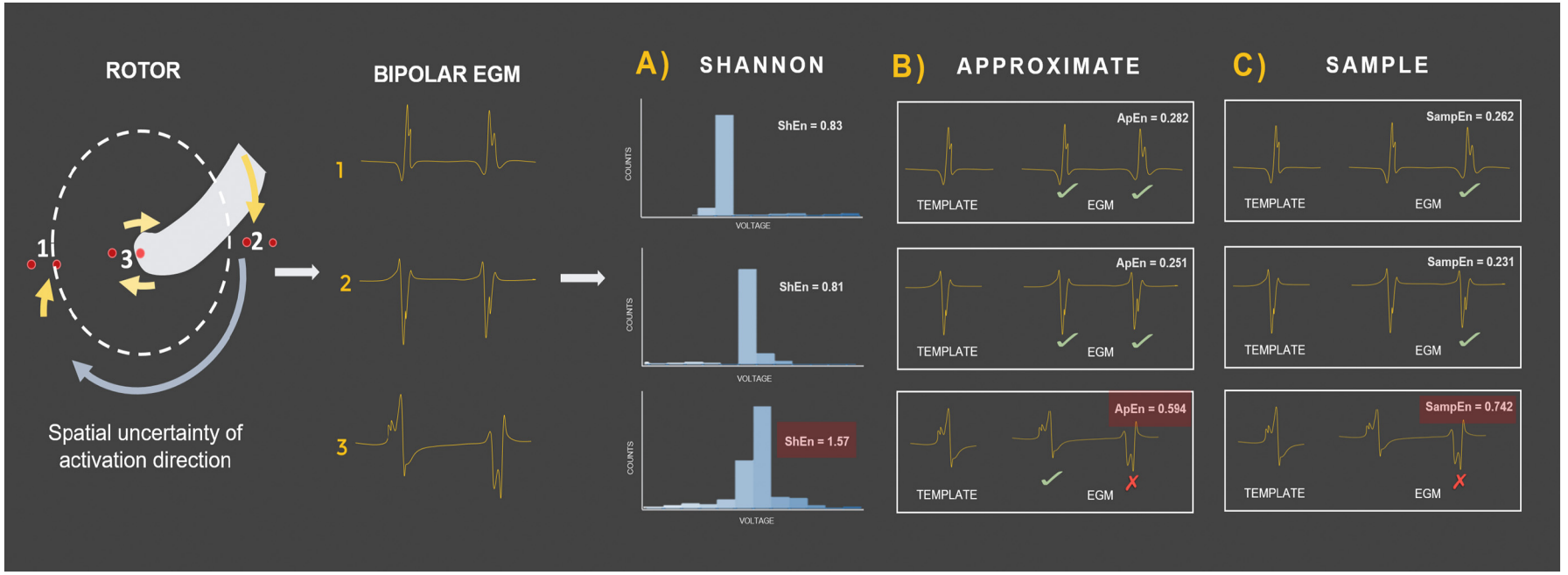

Fig. 1. High entropy correlates to the pivot of a spiral wave. An example of the relationship between entropy (ApEn, SampEn and ShEn) and a simple rotating wave, modified from Ganesan et al. [18]. Bipoles positioned in location 1 and 2 (at the periphery of the rotating wave) experience consistent activation direction, leading to more regular EGM morphology and a narrow amplitude histogram. Conversely, the bipole at position 3 (at the rotor pivot) experiences sharp local deflection, but secondary activity as the wavefront changes direction, including intermediate activity and an inverted potential. This uncertainty in wavefront activation direction can be quantified using entropy. In A) signal values are binned over a broader range of amplitudes, leading to higher ShEn. Contrastingly ApEn and SampEn are regularity metrics that identify the presence of repetitive patterns. B) Shows highest ApEn associated with signals with less repetitive patterns, and C) shows SampEn working in a similar fashion, though comparisons between a vector and itself are not included. This provides more accurate estimates of regularity. Note that high entropy is relative to what is being measured.

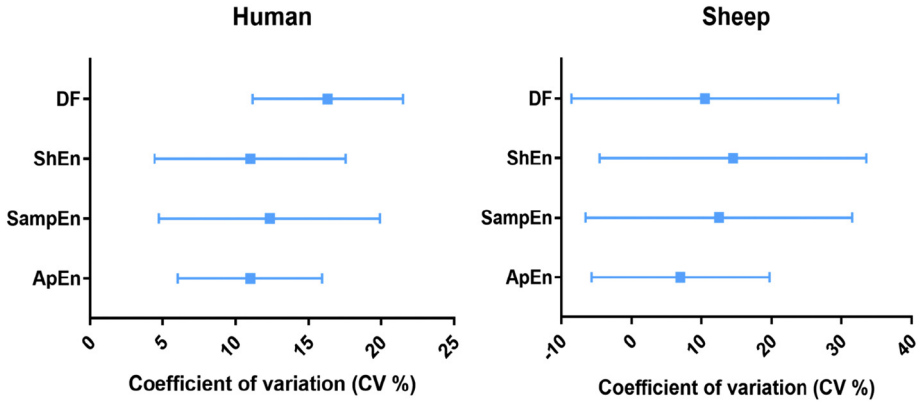

Fig. 2. CV for human and sheep patients. CV for human and sheep patients, which confirms dispersion of En values over time and is supportive of global temporal instability. The center square indicates mean CV over all sites, and the line SD. In humans, ApEn, SampEn and ShEn showed variability in entropy values over time in the posterior LA and Anterior LA. This was also seen in the RA. Similar findings were seen for sheep in both the Land RA.

provides a way to quantify information. Broadly speaking, entropy uses this concept to measure information content and as such, will be maximal for completely random systems [11,30]. AF mapping of rotors provides an interesting application of entropy, as several studies have demonstrated that the pivot of rotors experience spatial uncertainty in wavefront direction. This in turn generates bipolar EGM morphologies that are less predictable, which can be identified using entropy [19,24,31,32]. The concept of entropy is further discussed in Supplement S3.

In this study, entropy analysis was performed using three information theoretic measures: ShEn [30], ApEn [33] and SampEn [33], allowing for cross-validation of our findings. ShEn, ApEn and SampEn were estimated in 5 s windows for each bipolar electrode. For ShEn, samples were binned depending on their amplitude using a voltage histogram, with bin sizes dependent on the standard deviation (SD) of the signal (bin size $= 0.125 \times$ SD), as used in previous literature [19]. For ApEn and SampEn, we set an epoch length of $N = 5000$ (the window length at which to segment the data), a vector length $m = 2$ (finds matches of the same m voltage values within the sequence N) and a tolerance $r = 0.2 *$ SD (determines how often the following point $m + 1$ lies within tolerance r of matched vectors). The entropy algorithms are further detailed in Supplement S3.

To compare entropy to a more established mapping approach with previously explored temporal characteristics published in literature, dominant frequency (DF) analysis was performed as previously described (Supplement S5) [34]. The regularity index (RI) at each DF was obtained, and only DF possessing an RI > 0.2 were included in analyses. Code used for computation of DF is provided in Supplement S5.

Spatial coregistration

ApEn, SampEn, ShEn and DF values acquired for each anatomical region were superimposed onto the respective 3D electroanatomical map to assess temporal stability and spatial location.

Table 1
Human CV values by chamber.

Posterior LA		Anterior LA		RA	
ApEn	11.5% (95% CI, 7.2%, 15.8%)	*ApEn*	8.8% (95%CI, 6.8%, 10.9%)	*ApEn*	13.2% (95%CI, 7.7%, 18.6%)
SampEn	15.7% (95%CI, 10.9%, 20.9%)	*SampEn*	13.3% (95%CI, 10.3%, 16.4%)	*SampEn*	18.3% (95%CI, 11.7%, 24.9%)
ShEn	10.2% (95%CI, 7.2%, 13.9%)	*ShEn*	8.5% (95%CI, 5.7%, 11.3%)	*ShEn*	14.2% (95%CI, 11.4%, 16.9%)

Statistical analysis

To study the temporal stability of entropy, we utilised similar statistical analyses as previously published by Jarman [35] and Habel [26] to provide a multi-faceted approach to determine both the global stability of entropy and DF, as well as the relative stability of the highest entropy and DF regions.

First, the Friedman test was used to examine the global temporal stability of entropy and DF by ranking values in each 5-s window and looking at the differences in patterning across all segments [26] (Supplement S9, Fig. 5). $p < 0.05$ was used to infer inconsistent patterning and global instability. A simple explanation of how the Friedman test was performed is discussed in Supplement S9.

As a secondary analysis of global pattern stability, bootstrapping was implemented as described in Supplement S6. Bootstrapped matrices were used validate the observed p-values through comparison of an estimated distribution.

The relative stability of high entropy regions were studied using the kappa coefficient, which analysed the temporal stability of only the top 10% of entropy and DF [35]. Kappa coefficients were obtained by ranking entropy and DF in each 5 s segment, and evaluating the agreement in the presence and location of the top 10% of values across consecutive temporal segments (Supplement S10, Fig. 6). Consistent ranking of the top 10% of values in any given bipole was suggestive of relative temporal stability. A threshold of kappa >0.6 was used as a cut-off of stability, as used by Jarman [35]. Interpretations and a simple example for the kappa statistic are detailed in Supplement S10.

The coefficient of variation (CV) was also used to quantify the temporal variability of entropy and DF [26]. CV was calculated as a ratio of the standard deviation to the mean (SD/mean).

Results

Baseline characteristics of included patients are shown in Supplement S8. Multiple episodes of AF were analysed in humans (H: 26 epochs, duration: 6040 s) and sheep (S: 15 epochs, duration: 4160 s).

Global temporal instability of entropy

Entropy was found to change dynamically over time in medium to long-duration AF recordings, demonstrating global temporal instability. This was seen in both human and sheep models, and across all three entropy algorithms (ApEn, SampEn and ShEn). This dynamic change in entropy is clearly demonstrated in Movie 1 (Supplement S6), where the overall pattern of entropy is seen to exhibit flux and is not completely stable.

Table 2
Sheep CV values by chamber.

LA		RA	
ApEn	13.2% (95%CI, 7.7%, 18.6%)	*ApEn*	13.8% (95%CI, 6.9%, 20.7%)
SampEn	18.3% (95%CI, 11.7%, 24.9%)	*SampEn*	19.0% (95%CI, 10.6%, 27.4%)
ShEn	14.2% (95%CI, 11.4%, 16.9%)	*ShEn*	14.2% (95%CI, 10.5%, 17.9%)

Statistically, these findings were supported by the small Friedman test *p*-values. In the human cohort specifically, analysis demonstrated inconsistent global entropy patterns for ApEn, SampEn and ShEn over time the posterior LA (ApEn: $p < 0.001$; SampEn: $p < 0.001$; ShEn: $p < 0.01$), Anterior LA (ApEn: $p < 0.01$; SampEn: $p < 0.001$; ShEn: $p < 0.001$) and RA (ApEn: $p < 0.001$; SampEn: $p < 0.001$; $p < 0.01$). Additionally, the mean observed p-value ($P_{observed}$) fell within the 95% confidence interval (CI) of bootstrapped *p*-values ($P_{bootsrapped}$), supporting the presence of global temporal instability.

In sheep, Friedman test analysis results aligned with human findings, obtaining statistically significant p-values in the LA (ApEn: $p < 0.001$; SampEn: $p < 0.001$; ShEn: $p < 0.001$) and RA (ApEn: $p < 0.001$; SampEn: $p < 0.001$; ShEn: $p < 0.001$).This indicates inconsistent global patterning of entropy over time, and global temporal instability of ApEn, SampEn and ShEn. Observed p-values also fell within the 95% CI of bootsrapped p-values.

The CV also confirms the global temporal instability of entropy (Fig. 2). ApEn, SampEn and ShEn in humans showed a clear variability in entropy values over time in the posterior LA and Anterior LA. Similar values of coefficients of variation were seen in the RA (Table 1). Similar findings were seen for sheep in both the LA and RA (Table 2).

Relative temporal stability of the 10% of entropy

Despite the pattern of global flux, it was apparent that regions of highest entropy seemed to occur repetitively in the same location and exhibit relative temporal stability. This was demonstrated in both human and sheep models, and across all three entropy algorithms (ApEn, SampEn and ShEn) as demonstrated in Movie 1 (Supplement S6) and Fig. 3 and Fig. 4, where the regions of highest entropy (in blue and purple) occur consistently in the same anatomical location.

Kappa coefficients support this relative stability, with analysis of the top 10% of entropy in humans meeting the kappa stability cut-off of >0.6 in the posterior LA for ApEn (0.61 ± 0.32 (Median $\pm$ IQR)) and SampEn (0.65 ± 0.02). ShEn in this region was just below the cut-off (0.58 ± 0.35). In the anterior LA, kappa met the cut-off for all three algorithms (ApEn: 0.70 ± 0.38; SampEn: 0.61 ± 0.23; ShEn: 0.60 ± 0.39), as did kappa in the RA (ApEn: 0.66 ± 0.17; SampEn: 0.66 ± 0.16; ShEn: 0.65 ± 0.19). Findings were similar for the long-term sheep study, with kappa above 0.6 in the LA for ApEn (0.73 ± 0.22) and SampEn (0.68 ± 0.10), while ShEn yielded kappa just below the cut-off (0.59 ± 0.15). In the RA, all kappa met the 0.6 threshold (ApEn: 0.76 ± 0.22; SampEn: 0.74 ± 0.18; ShEn: 0.61 ± 0.27). Kappa distributions for human and sheep studies are summarized in Fig. 5.

Comparison of entropy temporal characteristics with DF

In both human and sheep models, DF demonstrated global temporal instability as reflected by the low p-values computed using the Friedman test (H: $p < 0.01$; S: $p < 0.01$). In addition, DF did not demonstrate a relative stability of the top 10% of DF in humans and yielded low kappa values (anterior LA: 0.09 ± 0.15; posterior LA: 0.18 ± 0.42; RA: 0.06 ± 0.11). The same was seen in the long-term sheep study (LA: 0.22 ± 0.22; RA 0.39 ± 0.30). Kappa values were also found to be similar to those previously published by Jarman.

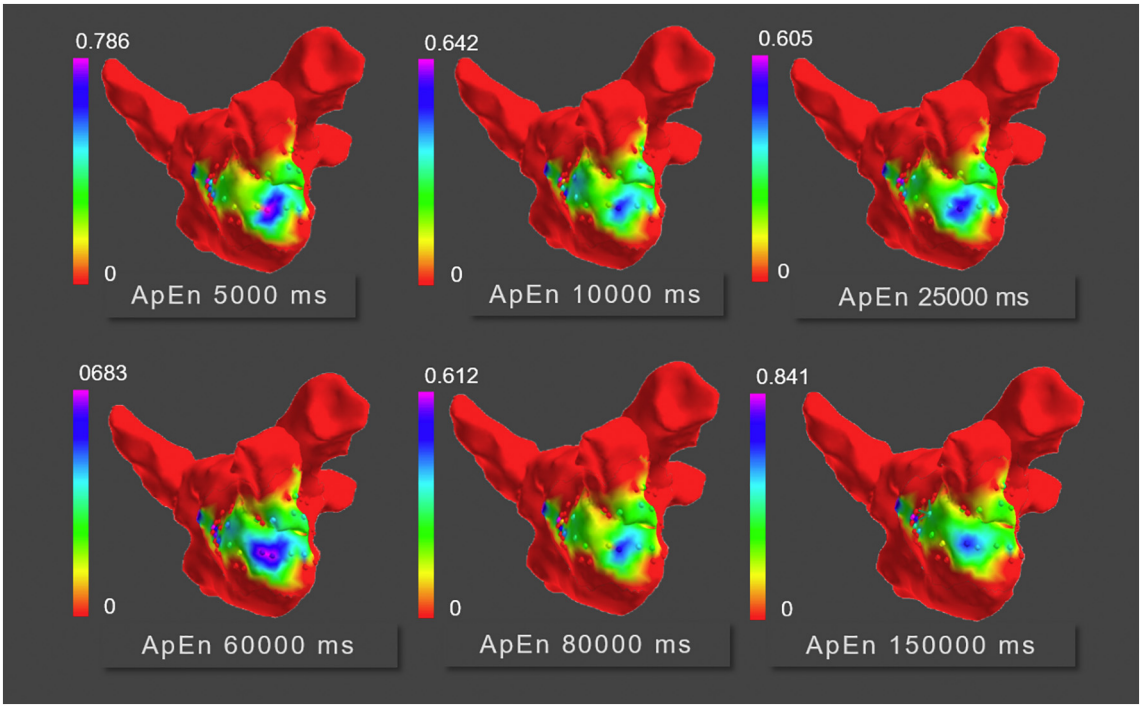

Fig. 3. Relative temporal stability of 10% entropy regions (human). This figure shows a basket recording in the anterior LA of a human patient in persistent AF. Each snapshot is representative of a 5-s segment of recording, with ApEn plotted by colour. Despite a pattern of global flux, it is apparent that the top 10% of ApEn (in blue and purple) occur repetitively at the same anatomical region. This suggests a relative stability of highest entropy. Kappa coefficients support this relative stability, with the top 10% of ApEn in humans meeting the kappa (reported as Median $\pm$ IQR) stability cut-off of >0.6 in the posterior LA (0.61 ± 0.32), anterior LA (0.70 ± 0.38) and RA (0.66 ± 0.17). (For interpretation of the references to colour in this figure legend, the reader is referred to the web version of this article.)

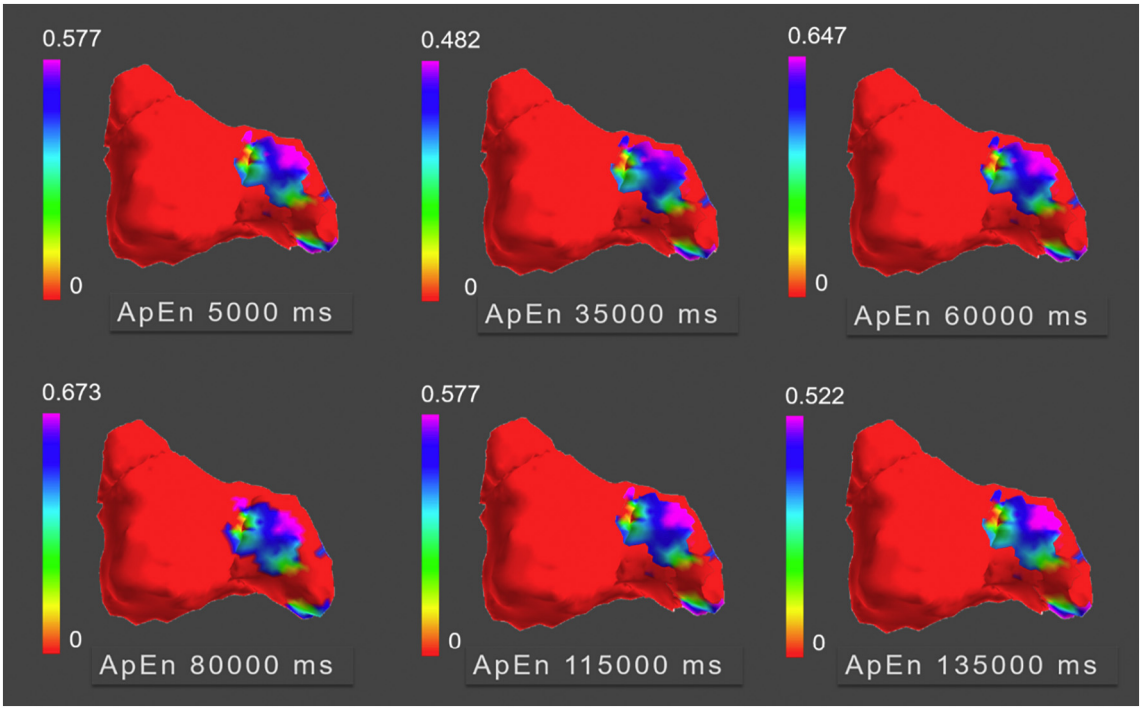

Fig. 4. Relative temporal stability of 10% entropy regions (sheep). This figure shows a basket recording in the LA of a sheep subject in tachypaced AF. Each snapshot is representative of a 5-s segment of recording, with ApEn plotted by colour. The long duration sheep study showed similar temporal characteristics as the human study, with the top 10% of ApEn (in blue and purple) occurring repetitively at the same anatomical region and exhibiting relative temporal stability. Statistically, this was reflected by kappa above 0.6 in both the LA (0.73 ± 0.22), and RA (0.76 ± 0.22). (For interpretation of the references to colour in this figure legend, the reader is referred to the web version of this article.)

When compared to entropy, DF consistently yielded lower Kappa across all entropy algorithms and across the two species, with one way Anova testing reflecting these significant differences (H: $p = 0.003$; S: $p = 0.001$) (Fig. 5).

Comparison of entropy temporal characteristics with computational simulations

To provide mechanistic insights into the potential AF mechanism responsible for the human and sheep temporal characteristics, we compared our findings with various wave propagation scenarios (Fig. 6). The characteristics of these were as follows:

(i) Planar wave conduction

For planar waves (Fig. 6A), bipolar EGM morphologies were uniform throughout the mapped region, producing homogeneous ApEn, SampEn, ShEn and DF maps and high temporal stability (Entropy-Kappa: 0.921; Friedman test: $p > 0.01$; DF- Kappa: 1.00. Friedman test: $p > 0.01$).

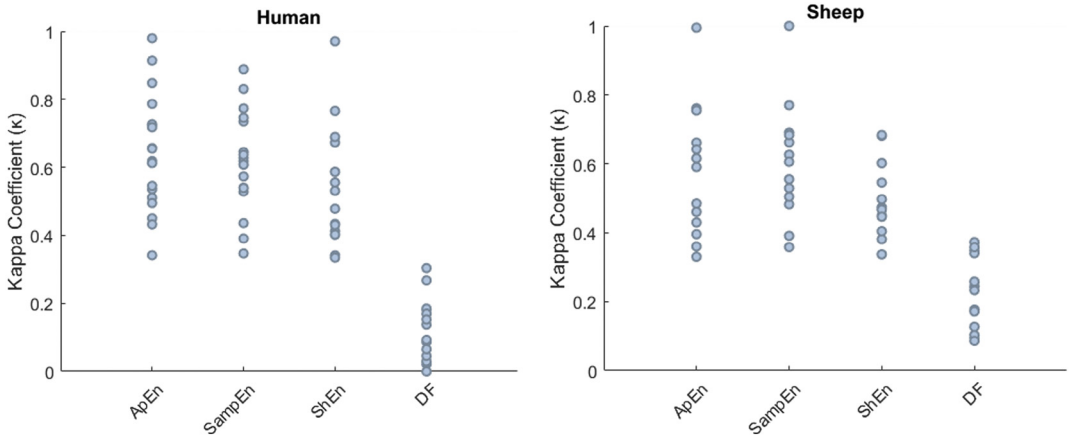

Fig. 5. Kappa distribution in humans and sheep. Scatter plot illustrating the distribution of Kappa across patients. For both species, DF did not demonstrate a relative stability of the top 10% of DF (H: anterior LA: 0.09 ± 0.15; posterior LA: 0.18 ± 0.42; RA: 0.06 ± 0.11; S: LA: 0.22 ± 0.22; RA 0.39 ± 0.30). Kappa across all entropy algorithms were consistently higher than for DF, with one way Anova testing showing significant differences between in humans ($p = 0.003$) and sheep ($p = 0.001$). DF Kappa values were similar to those previously published by Jarman [35].

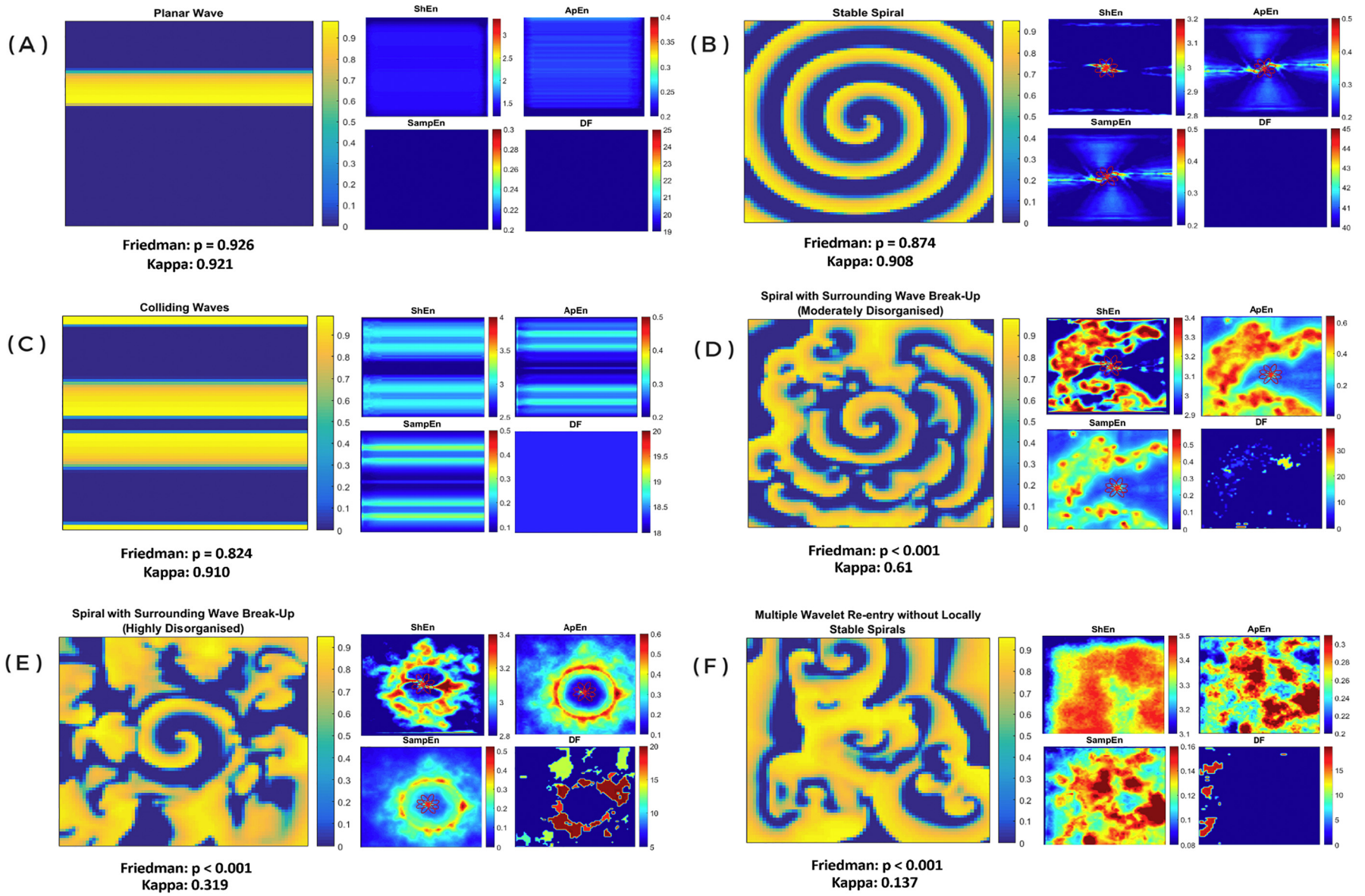

Fig. 6. Simulated AF cases representing various modes of wave propagation. Computer simulations representing various wave propagation patterns. Pivot points are marked with a red rosette. For A) all maps are uniform across mapped region, with high stability ($p > 0.01$; kappa: 0.921). B): ApEn, SampEn and ShEn demonstrate high entropy at the pivot, with high relative stability (kappa: 0.908) and global stability ($p > 0.01$). C): low ApEn, ShEn and SampEn were associated with collision zone, but there was high overall temporal stability ($p > 0.01$; kappa: 0.910). DF was uniform across mapped region. D) High ApEn, SampEn and ShEn were associated with regions of repetitive wave cross propagation and pivot. Temporal patterns showed global instability ($p < 0.001$) but relative stability of top 10% En (Kappa: 0.61). This model replicated human and sheep temporal characteristics best. E) High En was associated with regions of repetitive cross propagation and the pivot, but temporal stability was low overall ($p > 0.001$; kappa: 0.319). F): High ApEn, SampEn and ShEn were associated with regions of repetitive wave cross propagation, but temporal stability was very low overall ($p > 0.001$; kappa: 0.137). (For interpretation of the references to colour in this figure legend, the reader is referred to the web version of this article.)

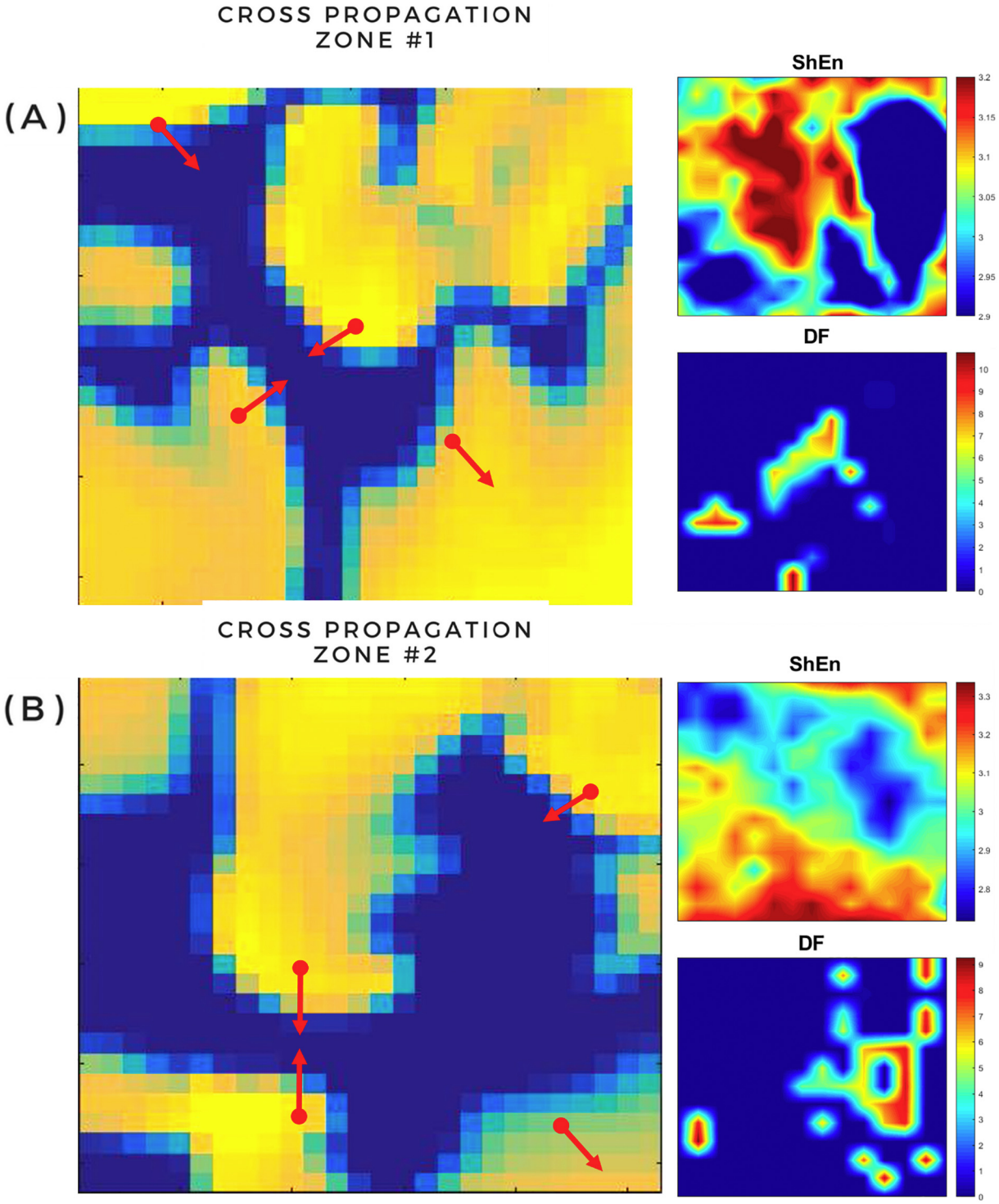

Fig. 7. High entropy is not specific to rotors, occurring also at sites of repetitive wave cross propagation.

(ii) Stable spiral wave (rotor)

Bipolar EGM exhibited deflections with less regular morphologies at the centre of the rotor, producing a stable region of high entropy at the pivot (Fig. 6B). As maximum entropy is consistently localized at the pivot, high relative temporal stability of the 10% En (Kappa: 0.908) and global temporal stability ($p > 0.01$) of entropy was observed. Contrastingly, DF showed no association with the rotor pivot and was uniform across the mapped region (Kappa: 1.00; Friedman test: $p > 0.01$).

(iii) Planar wave collision

In simulations depicting the head-on collision of waves (Fig. 6C), low ApEn, ShEn and SampEn were associated with the collision zone. The difference between the collision zone and surrounding areas was

ApEn: 0.08 nats; ShEn: 0.08 nats; SampEn: 0.03 nats. DF was uniform across the mapped region (18.4 Hz). High relative temporal stability (Kappa: 0.824) and global stability ($p > 0.01$) of entropy was observed.

(iv) Relatively stable spiral surrounded by highly disorganised spiral wave break-up.

Cases emulating a spiral surrounded by highly disorganised wave breakup (Fig. 6E) demonstrated low relative temporal stability of the top 10% of entropy and DF (Kappa: 0.319) and high global instability ($p < 0.0001$).

(v) Relatively stable spiral surrounded by moderately disorganised spiral wave break-up.

Contrastingly, a spiral surrounded by moderately disorganised wave breakup (Fig. 6D) reproduced human and animal results best, showing relative stability of the top 10% of entropy (Kappa: 0.610) but low global stability ($p < 0.001$). Like human and animal models, this model also produced top 10% DF regions with low stability (Kappa: 0.276; $p > 0.0001$). High entropy regions in these cases were associated with both the pivot and regions of repetitive cross propagation.

(vi) Multiple wavelet *re*-entry without locally stable spirals.

Disorganised wavelet re-entry (Fig. 6F) demonstrated low spatiotemporal stability of the top 10% of entropy and DF (Kappa: 0.137) and high global instability ($p < 0.0001$).

The Friedman and kappa statistics acquired for the model depicting a stable spiral surrounded by moderately disorganised wave breakup suggests that this may be the underlying AF mechanism responsible for the temporal characteristics of entropy seen in our human and sheep studies.

Specificity analysis of high entropy

High entropy was not specific to only rotors, with regions of repetitive wave cross propagation also associated with high entropy (Fig. 7). The entropy at the cross propagation zone was compared to surrounding planar propagation, with the difference equal to (ApEn: 1.75 nats $\pm$ 0.9, $p < 0.01$; ShEn: 0.75 nats $\pm$ 0.3, $p < 0.01$; SampEn: 2.5 nats $\pm$ 0.3, $p < 0.01$).

Qualitatively, high entropy regions were associated with interaction zones where waves repeatedly arrive from different directions, whilst high DF regions did not show association to such behaviour (Fig. 7).

Discussion

To date, the vast majority of electrogram stability studies have used sequential electroanatomic mapping, which is limited by the inherent spatiotemporal instability of AF. The use of stable basket recordings overcomes this, however, relatively few studies currently utilize this approach. One study, by Habel et al. [26], demonstrated high spatiotemporal variability in complex fractionated atrial electrograms (CFAE) in human AF using a contact basket over 5 min. Another by Jarman et al. [35] used a non-contact basket catheter to assess high-density DF spatiotemporal stability over prolonged recording periods, whilst Child et al. [36] used simultaneous panoramic recordings to assess the temporal stability of phase singularities (PS). Together, these studies have suggested a high degree of temporal instability of electrogram properties in sustained AF when mapped using DF, CFAE and PS, suggesting these regions are constantly migrating, making them potentially challenging to target for ablation. Although entropy provides an appealing new approach to targeted ablation, it remained unknown whether such approaches to mapping would exhibit similar characteristics of temporal instability, which would hinder clinical application. In addition, the specificity of entropy was also unknown, which is influential to the application of entropy clinically.

To address these gaps, we studied the temporal characteristics and specificity of entropy using three studies: a medium-duration human basket study, a long-duration tachypaced sheep basket study, and a computational AF study. The principal findings of these studies were:

- Global temporal instability of entropy
- Despite this global flux, there was a partial stability of the top 10% of entropy
- The temporal characteristics of entropy seen in humans and sheep were best modelled by a relatively stable rotational wave with surrounding wave breakup, suggesting that this may be the underlying AF mechanism
- Entropy was not specific to only rotors, however, occurring also at sites of repetitive wave cross propagation

A major strength of this study is that findings have been cross validated, not only across species, but also across multiple entropy algorithms, with comparison to DF, and with follow up analyses of computational simulations. Further, to counter issues of reproducibility that are common with many current AF mapping studies in the field, we also promote transparency with respect to the algorithms utilised, with a commitment for full disclosure of the raw data and code used, allowing study findings to be reproduced by others.

An important consideration in this study is the relationship of entropy to previous studies of CFAE and DF. The concept of CFAE ablation was introduced by Nademanee [6,37], and consisted of ablation of multi-component fractionated deflections with a voltage cut-off ≤0.15 mV. Using a systematic approach, high-rates of AF termination were achieved in the original study, and favorable clinical outcomes by some others. Conversely, other studies failed to reproduce the promising outcomes [38].

The entropy findings in this study potentially provide a unifying explanation for the divergent findings of CFAE literature. While high entropy is demonstrated to be an intrinsic property of the pivoting regions of rotors, it also occurs at regions of repetitive wave cross propagation. This dual explanation for electrogram entropy is consistent with previous qualitative studies of fractionation in optically mapped atrial monolayers [39]. It may also provide an explanation of the divergent clinical results of CFAE ablation, with AF termination a repeatable observation at sites of fractionation (presumably driver regions with high entropy), but clearly lacking specificity (perhaps regions of wave cross propagation, also high entropy).

In regards to DF, this study closely reproduced previous findings suggesting spatiotemporal instability of bipolar EGMs in AF [26]. The seminal original studies of DF were carried out with analysis of optically mapped action potentials in cholinergically stimulated sheep AF [13]. The repetitive wave-like morphology of these signals is ideal for phase and spectral analysis, in contrast to the multi-component complex morphology of bipolar EGMs in AF [40]. When studied clinically, it has been difficult to demonstrate that DF based ablation leads to AF termination [41] or improved clinical outcomes [10]. The temporal instability of bipolar EGM-based measures of DF encountered in our study and others [26,35], is consistent with clinical data presented thus far.

Implications for future studies and clinical AF mapping

These results suggest that entropy-based approaches are a potentially appealing avenue for targeted ablation strategies in the future. Before clinical application however, methods of delineating rotors and regions of cross propagation are needed. This may be achieved in future via the use of machine learning algorithms that utilize other electrogram features, in addition to entropy, to differentiate between these two modes of wave propagation.

In addition, these findings lay the foundation for future studies exploring the statistical properties of bipolar electrograms in human AF.

The approach taken in our study, with primary analysis of AF EGM properties followed by exposition with computer simulations to provide inference, is rare thus far in the field.

Study limitations

Using the bipolar electrogram-based approach in the current study, we were unable to make direct inferences about wave propagation. There is no consensus fiducial point for myocardial electrical activation with the bipolar EGM [42], with its complex nature precluding direct annotation of activation timing. The study as such, does not provide an overall comprehensive explanation of the AF mechanism, with the links to potential wave propagation mechanisms being inferred instead. Nonetheless, we believe that the nuanced findings will be reproducible by others, and suggest a potential future direction to AF statistical signal processing studies.

Conclusion

This study demonstrates the presence of global temporal instability of entropy. However, within this instability there is relative stability of the top 10% of entropy, which may prove a potentially attractive ablation target in the future. Despite this, high entropy regions were associated with not just the pivot of spiral waves, but also regions of repetitive cross propagation, suggesting there may be multiple mechanisms capable of giving rise to high entropy. This suggests that methods of differentiating rotors and areas such as cross propagation are needed in future before application of entropy-based of approaches to clinical ablation is possible.

Supplementary data to this article can be found online at https://doi.org/10.1016/j.jelectrocard.2018.11.014.

Acknowledgement of funding

This work was supported by the National Health and Medical Research Council of Australia Project Grant (1063754) and National Heart Foundation of Australia (101188).

Computer simulation demonstrated an association between high En and cross propagation regions. At such sites, waves arrive from different directions (indicated by arrow), creating spatial uncertainty in activation direction similar to what is seen for rotors. The entropy at the cross propagation zone was compared to surrounding planar propagation, with the difference equal to ApEn: 1.75 nats $\pm$ 0.9, $p < 0.01$; ShEn: 0.75 nats $\pm$ 0.3, $p < 0.01$; SampEn: 2.5 nats $\pm$ 0.3, $p < 0.01$. These regions were associated with high entropy, but not DF.

References

[1] Clarnette JA, et al. Outcomes of persistent and long-standing persistent atrial fibrillation ablation: A systematic review and meta-analysis EP Europace ; 2017.
[2] Verma A, Macle L, Sanders P. Catheter ablation for persistent atrial fibrillation. N Engl J Med 2015;373(9):878–9.
[3] Calkins H, et al. 2017 HRS/EHRA/ECAS/APHRS/SOLAECE expert consensus statement on catheter and surgical ablation of atrial fibrillation. Heart Rhythm 2017;14(10):e275–444.
[4] Baumert M, Sanders P, Ganesan A. Quantitative-electrogram-based methods for guiding catheter ablation in atrial fibrillation. Proc IEEE 2016;104(2):416–31.
[5] Buch E, Mandapati R. The continuing search for patient-specific atrial fibrillation ablation targets: need for rigorously verified and independently replicated data. Heart Rhythm 2016;13(12):2331–2.
[6] Nademanee K, et al. A new approach for catheter ablation of atrial fibrillation: mapping of the electrophysiologic substrate. J Am Coll Cardiol 2004;43(11):2044–53.
[7] Narayan SM, et al. Treatment of atrial fibrillation by the ablation of localized sources: CONFIRM (conventional ablation for atrial fibrillation with or without focal impulse and rotor modulation) trial. J Am Coll Cardiol 2012;60(7):628–36.
[8] Benharash P, et al. Quantitative analysis of localized sources identified by focal impulse and Roter modulation mapping in atrial fibrillation. Circ Arrhythm Electrophysiol 2015;8:554–61.
[9] Verma A, et al. Approaches to catheter ablation for persistent atrial fibrillation. N Engl J Med 2015;372(19):1812–22.
[10] Atienza F, et al. Comparison of radiofrequency catheter ablation of drivers and circumferential pulmonary vein isolation in atrial fibrillation: a noninferiority randomized multicenter RADAR-AF trial. J Am Coll Cardiol 2014;64(23):2455–67.
[11] Dharmaprani D, et al. Information theory and atrial fibrillation (AF): a review. Front Physiol 2018;9.
[12] Jalife J, et al. Mechanisms of atrial fibrillation: mother rotors or multiple daughter wavelets, or both? J Cardiovasc Electrophysiol 1998;9(8 Suppl):S2–12.
[13] Skanes AC, et al. Spatiotemporal periodicity during atrial fibrillation in the isolated sheep heart. Circulation 1998;98(12):1236–48.
[14] Mandapati R, et al. Stable microreentrant sources as a mechanism of atrial fibrillation in the isolated sheep heart. Circulation 2000;101(2):194–9.
[15] Allessie MA, Bonke F, Schopman F. Circus movement in rabbit atrial muscle as a mechanism of tachycardia. II. The role of nonuniform recovery of excitability in the occurrence of unidirectional block, as studied with multiple microelectrodes. Circ Res 1976;39(2):168–77.
[16] Vakkuri A, et al. Time-frequency balanced spectral entropy as a measure of anesthetic drug effect in central nervous system during sevoflurane, propofol, and thiopental anesthesia. Acta Anaesthesiol Scand 2004;48(2):145–53.
[17] Ocak H. Automatic detection of epileptic seizures in EEG using discrete wavelet transform and approximate entropy. Expert Syst Appl 2009;36(2):2027–36.
[18] Ganesan AN, et al. Bipolar electrogram shannon entropy at sites of rotational activation: implications for ablation of atrial fibrillation. Circ Arrhythm Electrophysiol 2013;6(1):48–57.
[19] Ganesan AN, et al. Origin and characteristics of high Shannon entropy at the pivot of locally stable rotors: insights from computational simulation. PLoS One 2014;9(11):e110662.
[20] Aronis KN, Ashikaga H. Impact of number of co-existing rotors and inter-electrode distance on accuracy of rotor localization. J Electrocardiol 2018;51(1):82–91.
[21] Li C, et al. The spatiotemporal stability of dominant frequency sites in in-silico modeling of 3-dimensional left atrial mapping of atrial fibrillation. PLoS One 2016;11(7):e0160017.
[22] Orozco-Duque, A., et al., Approximate entropy can localize rotors, but not ectopic foci during chronic atrial fibrillation: A simulation study.
[23] Ugarte JP, et al. Dynamic approximate entropy electroanatomic maps detect rotors in a simulated atrial fibrillation model. PLoS One 2014;9(12):e114577.
[24] Arunachalam SP, F. PA, Mulpuru SK, Tolkacheva EG. Novel entropy approach to identify the core of the rotors in Atrial fibrillation. University of Minessota: Institute of Engineering in Medicine; 2014.
[25] Balasundaram K, et al. Tracking rotors with minimal electrodes: modulation index-based strategy. Circ Arrhythm Electrophysiol 2015;8(2):447–55.
[26] Habel N, et al. The temporal variability of dominant frequency and complex fractionated atrial electrograms constrains the validity of sequential mapping in human atrial fibrillation. Heart Rhythm 2010;7(5):586–93.
[27] Tedrow UB, Stevenson WG. Recording and interpreting unipolar electrograms to guide catheter ablation. Heart Rhythm 2011;8(5):791–6.
[28] ten Tusscher KH, Panfilov AV. Alternans and spiral breakup in a human ventricular tissue model. Am J Physiol Heart Circ Physiol 2006;291(3):H1088–100.
[29] Welch P. The use of fast Fourier transform for the estimation of power spectra: a method based on time averaging over short, modified periodograms. IEEE Trans Audio Electroacoust 1967;15(2):70–3.
[30] Shannon C. A mathematical theory of communication. Bell Syst Tech J 1948;27:379–423 [623–656].
[31] Ganesan AN, et al. Bipolar electrogram shannon entropy at sites of rotational activation: implications for ablation of atrial fibrillation. Circ Arrhythm Electrophysiol 2012;6:48–57 [p. CIRCEP. 112.976654].
[32] Orozco-Duque A, et al. Approximate entropy can localize rotors, but not ectopic foci during chronic atrial fibrillation: A simulation study. Computing in Cardiology Conference (CinC), 2013. IEEE; 2013.
[33] Richman JS, Moorman JR. Physiological time-series analysis using approximate entropy and sample entropy. Am J Physiol Heart Circ Physiol 2000;278(6):H2039–49.
[34] Sanders P, et al. Spectral analysis identifies sites of high-frequency activity maintaining atrial fibrillation in humans. Circulation 2005;112(6):789–97.
[35] Jarman JW, et al. Spatiotemporal behavior of high dominant frequency during paroxysmal and persistent atrial fibrillation in the human left atrium. Circ Arrhythm Electrophysiol 2012;5(4):650–8.
[36] Child N, et al. Unraveling the underlying arrhythmia mechanism in persistent atrial fibrillation: results from the STARLIGHT study. Circ Arrhythm Electrophysiol 2018;11(6):e005897.
[37] Nademanee K, Oketani N. The role of complex fractionated atrial electrograms in atrial fibrillation ablation moving to the beat of a different drum. J Am Coll Cardiol 2009;53(9):790–1.
[38] Oral, H., et al., A randomized assessment of the incremental role of ablation of complex fractionated atrial electrograms after antral pulmonary vein isolation for long-lasting persistent atrial fibrillation. J Am Coll Cardiol, 2009. 53(9): p. 782–9.
[39] Umapathy K, et al. Electrogram fractionation in murine HL-1 atrial monolayer model. Heart Rhythm 2008;5(7):1029–35.
[40] Wells Jr JL, et al. Characterization of atrial fibrillation in man: studies following open heart surgery. Pacing Clin Electrophysiol 1978;1(4):426–38.
[41] Verma A, et al. Relationship between complex fractionated electrograms (CFE) and dominant frequency (DF) sites and prospective assessment of adding DF-guided ablation to pulmonary vein isolation in persistent atrial fibrillation (AF). J Cardiovasc Electrophysiol 2011;22(12):1309–16.
[42] Biermann M, S. M, Borggrefe M, Hindricks G, Haverkamp W, Breithardt G. The interpretation of cardiac electrograms. In: Shenasa MB, M, Breithardt G, editors. Cardiac mapping. Blackwell; 2003. p. 15–39.